Accepted Manuscript

Engineering of keratin functionality for the realization of bendable all-biopolymeric micro-electrode array as humidity sensor

M. Natali, A. Campana, T. Posati, E. Benvenuti, F. Prescimone, D.O. Sanchez Ramirez, A. Varesano, C. Vineis, R. Zamboni, M. Muccini, A. Aluigi, S. Toffanin

Please cite this article as: Natali, M., Campana, A., Posati, T., Benvenuti, E., Prescimone, F., Ramirez, D.O.S., Varesano, A., Vineis, C., Zamboni, R., Muccini, M., Aluigi, A., Toffanin, S., Engineering of keratin functionality for the realization of bendable all-biopolymeric micro-electrode array as humidity sensor, *Biosensors and Bioelectronics* (2019), doi: https://doi.org/10.1016/j.bios.2019.111480.

Engineering of keratin functionality for the realization of bendable all-biopolymeric micro-electrode array as humidity sensor

M. Natali*[a], A. Campana[a], T. Posati[b], E. Benvenuti[a], F. Prescimone[a], D.O. Sanchez Ramirez[c], A. Varesano[c], C. Vineis[c], R. Zamboni[b], M. Muccini[a], A. Aluigi[b], S. Toffanin*[a]

[a] Consiglio Nazionale delle Ricerche (CNR)— Istituto per lo Studio dei Materiali Nanostrutturati (ISMN), Via P. Gobetti 101, 40129 Bologna, Italy
[b] Consiglio Nazionale delle Ricerche (CNR)— Istituto per la Sintesi Organica e la Fotoreattività (ISOF), Via P. Gobetti 101, 40129 Bologna, Italy
[c] Consiglio Nazionale delle Ricerche (CNR), Istituto di Sistemi e Tecnologie Industriali Intelligenti per il Manifatturiero Avanzato (STIIMA), Corso Giuseppe Pella 16, 13900 Biella, Italy

emails: mnatali@ismn.cnr.it (Marco Natali), stefano.toffanin@cnr.it (Stefano Toffanin)

Abstract

The technological quest for flexible devices to be interfaced with the biological world has driven the recent reinvention of bioderived polymers as multifunctional active and passive constituent elements for electronic and photonic devices to use in the biomedical field. Keratin is one of the most important structural proteins in nature to be used as biomaterial platform in view of the recently reported advances in the extraction and processing from hair and wool fibers. In this article we report for the first time the simultaneous use of naturally extracted keratin as both active ionic electrolyte for water ions sensing and as bendable and insoluble substrate into the same multielectrode array-based device. We implemented the multifunctional system exclusively made by keratin as a bendable sensor for monitoring the humidity flow.
The enhancement of the functional and structural properties of keratin such as bendability and insolubility were obtained by unprecedented selective chemical doping. The mechanisms at the basis of the sensing of humidity in the device were investigated by cyclic voltammetry and rationalized by reversible binding and extraction of water ions from the volume of the keratin active layer, while the figures of merit of the biopolymer such as the ionic conductivity and relaxation time were determined by means of electrical impedance and dielectric relaxation spectroscopy. A reliable linear correlation between the controlled-humidity level and the amperometric output signal together with the assessment on measure variance are demonstrated. Collectively, the fine-tuned ionic-electrical characterization and the validation in controlled conditions of the free-standing insoluble all-keratin made microelectrode array ionic sensor pave the way for the effective use of keratin biopolymer in wearable or edible electronics where conformability, reliability and biocompatibility are key-enabling features.

Keywords: biopolymers, keratin, bendable, micro-electrode array, humidity sensor

1. Introduction

Biocompatible, flexible and stable materials able to transduce biochemical responses into electrical signals are of fundamental interest to produce electrochemical sensors capable to adapt to the irregular surface of the biological constructs. Expanding the set of non-toxic materials suitable to fabricate electronic and photonic devices allows to design multifunctional platforms

1 that can be implemented for neural stimulation and recording (Benfenati et al., 2013; Toffanin et
2 al., 2013), label-free optical detection (Toffanin et al., 2012) or regenerative medicine (Agarwala
3 et al., 2018). Among various gas/vapor sensing electrochemical materials (Deng, 2013; Li, 2018;
4 Zhou et al., 2018), intrinsically conducting biopolymers offer not only the strictly-needed
5 biocompatibility but also the chance to engineer transducing systems with electronic and ionic
6 transport properties (Robinson et al., 2017; Wünsche et al., 2015).

7 Among the others, keratins extracted from wool- and human hair are a complex and critical class
8 of biopolymers at high technological potential. Indeed, they show to form self-assembled
9 arrangements for regulating cellular recognition and behavior (Rouse and Van Dyke, 2010), for
10 wound healing (Aluigi et al., 2015; Tang et al., 2012), drug delivery (Cheng et al., 2018; Cilurzo
11 et al., 2013) and tissue engineering (Baker et al., 2017; Tachibana et al., 2002). However, the
12 major advantages of keratin biopolymers are appropriate filmability and low superficial
13 roughness, high transparency, low temperature processing and the use of fully water-based
14 extraction   solvent,   which   are   fundamental   characteristics   for   fabricating
15 biocompatible/biodegradable sensors. Furthermore, keratin extracted from wool belongs to
16 waste products generated in large quantities from food industries, especially slaughterhouse,
17 dairy and poultry industry so that its recovery and valorization provide low-impact solutions
18 with respect to conventional solid electrolytes.

19 In the present paper, we identify keratin as a remarkable bioderived polymer capable to display
20 multifunctional properties to be used simultaneously in biosensors as both active material for
21 ionic/electrical transduction and layer for free-standing insoluble and bendable substrate. We
22 highlight the relevant application field of the all-keratin biosensor is humidity/respiratory
23 monitoring. As it is extensively reported in literature (M. Folke et al, 2003), there is an urge
24 need to define new methods capable to provide humidity measure in a non-obtrusive fashion
25 while being intelligent, selective, adaptive, contactless and fast responding. Indeed, keratin
26 biopolymer is considered an excellent candidate to sense humidity since the hydrogen and
27 hydroxyl ions (H^+ and OH^-) formed by water dissociation are expected to drift under the
28 influence of the applied electric field. The keratin chains tend to organize into a crystalline α-
29 helix structures, and form H-bonded water network with amino acids groups on its side chains
30 able to support proton transfer under high humidity (Hamouche et al., 2018; Miyake and
31 Rolandi, 2016).

32 However, the keratin-based sensor must guarantee the multiple use in aqueous environment
33 without dissolving for continuous and reliable operation. The novel approach that we propose
34 for enhancing the structural/functional properties of keratin biopolymer is based on selective
35 chemical doping. Here, we report on the addition of glutaraldehyde by simple immersion
36 process for achieving insolubility of the processed keratin film. Moreover, the further addition of
37 glycerol enables the use of the doped biopolymer as a bendable, biocompatible and transparent
38 substrate for sensing applications while preserving the mechanical stability of pure keratin.

39 We validate for the first time the use of keratin as both multifunctional biomaterial and device
40 platform for the engineering of a bendable free-standing multielectrode array for monitoring the
41 humidity flow in controlled conditions.

42 The hygroscopic properties of pristine wool keratin are preserved in the thin-film form and the
43 linear correlation between the output electrical signal of the Keratin-based Bipole (KBs) devices
44 and the environmental humidity levels is demonstrated.

45 Considering the ion transport and collection in the bulk of the active material and the proton
46 collection at the interfaces with the electrodes as the factors limiting the transduction
47 performance of the sensor, a possible optimization strategy is explored (i) by blending keratin
48 and melanin biopolymer for obtaining a higher ion-conductivity composite and (ii) by
49 integrating palladium electrodes passivated with hydrogen (PdHx)into the sensor architecture to
50 efficiently extract/inject protons.

In the current scenario of the plethora biocompatible humidity sensors based on different transduction mechanisms (Hamouche et al., 2018), the function-selective chemical processing of the bioderived keratine enables the realization of a conformable multielectrode array system that (i) is completely made by a single biopolymer, (ii) can be twisted while retaining mechanical stability, (iii) is preserved in air and liquid environments over several days and (iv) can provide a reliable, stable and calibrated amperometric output signal.

2. Materials & Methods

2.1. Keratin thin film fabrication and characterization

Keratin solutions are made by dissolving extracted keratin from wool fibers at concentrations 10% (w/v) in aqueous solvent. Further details on the biopolymer extraction are described in other published work (Posati et al., 2018). The obtained solutions are centrifuged at 4000 rpm for 10 minutes. The glass/ITO substrates are washed three times in acetone and isopropanol in ultrasonic bath before a plasma treatment in O_2 environment at 200 W for 180 s in ISO7 cleanroom facility. Thin films of keratin are fabricated by spin coating filtered keratin solutions on glass/ITO substrates at 1000 rpm for 180 s with acceleration of 200 rpm/s. Subsequently, another step at 3000 rpm and acceleration of 1000 rpm/s is added to form homogeneous surfaces. The films are then dried in ambient at room temperature for at least 24 h and stored in inert atmosphere glovebox. The diode-like KB is realized by sandwiching the keratin thin film between the Indium Tin Oxide (ITO) and gold electrodes in a vertical architecture. Instead, in the coplanar KB architecture, two gold electrodes separated by a 70-µm-wide channel are deposited on top of the substrate/keratin active layer. Gold is deposited under high vacuum at a base pressure of 10^{-6} mbar at a growth rate of 0.1 nm/s. The storage of moisture is revealed by collecting electrical current of the sensor. Reversible infilling and removal of H^+/OH^- ions from the sensor active layer volume are probed by performing cyclic voltammetry in an environmental chamber with controlled relative humidity (RH) monitored with a traceable hygrometer. Film thickness is determined by measuring the step height of a scratch test using a stylus profilometer (KLA-Tencor P-7) and the film roughness is measured by atomic force microscopy (NT-MDT Spectrum Instruments). Image of the surface of the keratin thin-film deposition is reported in Figure S1 in Supporting Information. The superficial roughness (Root-Mean-Square Height) determined by topographical measurement is around 1-2 nm: the smooth keratin-film surface allows the deposition of homogenous and compact metal electrode thus avoiding possible shortcuts with the ITO electrode
Insoluble keratin thin films are obtained by immersion in glutaraldehyde overnight.
The overall value-chain from the extraction of keratin protein to the realization of the keratin-based devices for humidity-sensing is reported in Figure S2 in Supporting Information.

2.2. Keratin doping by melanin biopolymer

Melanin solutions are made by dissolving lyophilized melanin powder extracted from yak fibers at concentration of 28 mg/mL in H_2O/NH_3 (1:2). Melanin is extracted by hydrolysis at 105 °C with HCl 6N in 24 h. The keratin-melanin composite films are prepared by mixing the aqueous keratin and melanin solutions in order to have a melanin concentration of 9% wt vs keratin. Thin films are then fabricated by spin coating filtered solutions on glass/ITO substrates following the same protocol as for keratin thin film reported above.

2.3. Free-standing array of KB sensors

Free-standing keratin substrates are prepared from pure keratin solution by adding glycerol (25% wt vs keratin), and 0.4 μL of glutaraldehyde (25% wt) per mg of keratin. Then, a thin film of pure keratin is spin-coated by using the same parameters reported above to fabricate biopolymer thin film on glass/ITO substrates. The microelectrode array is fabricated by using gold electrode sublimation in a thermal evaporator under high vacuum at base pressure of 10^{-6} mbar and growth rate of 0.1 nm/s. The channel is maintained 70-nm-wide as in the KB sensors.

2.4. Protodes fabrication

The protodes fabrication is optimized into a portable glove box (Bel-Art) equipped with inlet flow stream to connect hydrogen gas (AZOIDRO mixture: 95% Nitrogen and 5% Hydrogen) and outlet flow stream to adjust the internal partial pressure. Internal RH is monitored with a traceable hygrometer (Fisher Scientific). The palladium electrodes are thermally sublimed under high vacuum at base pressure of 10^{-6} mbar and growth rate of 0.1 nm/s, then the absorption of H_2 from the glove box environment occurs spontaneously to create PdH_x protodes. We monitor the functionalization process through cyclic voltammetry observing the rise of the currents after 3-5 s.

2.5. Cyclic voltammetry of keratin thin films

Cyclic voltammetry (CV) experiments are performed in potentiostatic mode with a two-electrode electrochemical cell on Autolab PGSTAT 128N Electrochemical Analyzer (USA METROHM Company). In the diode-like KB sensor the keratin-coated ITO electrode served as the working electrode while the top gold electrode serves as the counter electrode. Instead, in coplanar KB sensor the electrodes are interchangeable due to the symmetry of the system. We performed single-cycle CV curves as preliminary and rapid electrical test to verify the sensor current-dependence as a function of humidity absorption. Then, multiple-cycle CV curves were collected with 4 cycles per measurement. An environmental chamber (MEMMERT HCP 153) is used to set a constant temperature emulating the human body (36 °C) and a variable RH% monitored with a traceable hygrometer (Fisher Scientific). I-V sweeps were performed, if not otherwise specified in the plot, at scan rate of 0.1 V/s.
Additionally, in order to provide information about the repeatability of the sensing performance of the different devices, we characterized 3 device samples for each architecture (i.e. soluble vertical diode-like KB sensors, insoluble vertical diode-like KB sensors and free-standing keratin-based microelectrode array) that are measured at constant RH 60% in order to determine standard errors to be associated to the data plotted in CV and Electrochemical Impedance Spectroscopy (EIS) curves reported in Figures 1, 2, 3c, 4, 5c.

3. Results and Discussion

3.1. Soluble diode-like KB sensors

We fabricated the keratin thin-film to be used as sensor active layer by means of spin coating process on top of the ITO-coated glass substrate following the protocol described in the

1 Materials & Methods section. In Figure 1a the cyclic voltammetry curves are shown. We
2 performed single-cycle CV curve at constant scan rate onto hydrated keratin thin-films in
3 ambient air at different acquisition times after one-night storage in inert atmosphere as initial
4 screening. The curve shape indicates a relevant time-dependent hysteresis loop expansion due to
5 introduction of water molecules, as already observed in other biopolymers (Ambrico et al., 2011;
6 Cicco et al., 2015; Evans et al., 2003; Zhong et al., 2011). Figure S3 in Supporting Information
7 shows the capacitive origin of the observed displacement current which has to be added to the
8 resistive component. Indeed, when the voltage scan rate is increased at constant air humidity and
9 applied potential V, we observe a current increase. Accordingly, by keeping constant the voltage
10 scan rate and the air humidity, the current I is enhanced by increasing the maximum potential V
11 applied to the bottom and top electrode of the KB sensor vertical architecture.
12 These observations are described by the general expression reported below:
13

$$I = \frac{\partial Q}{\partial t} = \frac{\partial (CV)}{\partial t} = V \frac{\partial (C)}{\partial t} + C \frac{\partial (V)}{\partial t} \qquad (1)$$

14
15 The first addendum in (1) is related to capacitance (C) variation related to trapping or de-
16 trapping of water molecule in keratin layers (Murphy, 1976) due to ambient humidity. The
17 second addendum in (1) describes the current variation dependence from the scan rate changes
18 during the electrical measurement.
19 We perform electrochemical spectroscopy impedance (EIS) in ambient air humidity in order to
20 model the electrical behavior of the keratin thin-film. The shape of the Nyquist plots shown in
21 Figure 1a compares favorably to those originated for other ion-conducting materials (Hod et al.,
22 2015; Ordinario et al., 2014; Wünsche et al., 2015; Yadav and Fedkiw, 2012) with high
23 reproducibility among different device samples (Figure S2 in Supporting Information). As
24 reported elsewhere (Lago et al., 2018, 2016), EIS characterization method allows us to describe
25 the whole hydrated system by electrical equivalent circuit and to extract significant figures of
26 merit as the ionic conductivity of the biopolymer. The electrical equivalent circuit that best fits
27 the experimental data is reported in the inset of Figure 1b. The fitting parameters are reported in
28 Table S1 in Supporting Information The equivalent circuit chosen from literature to model the
29 solid polymeric electrolyte (Qian et al., 2001) shows excellent agreement with respect to
30 experimental data, with a χ-squared value of 0.002. Moreover, the extrapolated geometry
31 capacity value C_g is comparable to the measurements outperformed in the same experimental
32 conditions with a capacitance meter. The other extrapolated parameters are R_b representing the
33 bulk ionic resistance of the keratin film, the Constant Phase Element (CPE_1) describing the
34 features of the double layer forming between the electrolyte and the electrode interface and
35 CPE_2 describing the effects of dipolar relaxation. The high-frequency semicircle reflects the
36 combination of R_b, C_g and CPE_2, while the straight line subsequent to the semicircle can be
37 correlated to the double layer capacity of an inhomogeneous electrode surface, and so to CPE_1
38 (Qian et al., 2001). Moreover, we introduced CPE_3 as an extra variable with respect to the
39 literature to take in consideration the asymmetry between the ITO and gold electrodes which
40 may cause variability in the double layer capacitance.
41 In order to asses the correlation between the sensing KB device output and the environment
42 humidity, an environmental chamber with controlled RH monitored with a traceable hygrometer
43 is used. The humidity-dependent Nyquist plots and the direct-current measurements are shown
44 in Figure 2. The shape of the Nyquist plots remains unchanged with respect to air-humidity
45 conditions, but we clearly observe the high-frequency semicircle reduction (Figure 2a and
46 Figure S5 in Supporting Information) thus indicating a corresponding drop of the R_b bulk ionic
47 resistance.
48 The ionic conductivity is calculated from Equation (2) as:

1

$$\delta = \frac{d}{R_b S} \qquad (2)$$

2

3   where d represents the film thickness (which is 450±10 nm according to profilometry
4   measurements), R_b the bulk ionic resistance extrapolated from EIS fitting procedure and S the
5   electrode area, i.e. 6 mm^2. The humidity-dependent ionic conductivity and the parameters used
6   for its calculation are reported in Table 1.
7   The increased ionic conductivity demonstrates that the uptake of water leads to more efficient
8   percolative pathways for ion hopping due to the increase in the H bonds in the keratin backbone
9   (Miyake and Rolandi, 2016). The RH is limited to 80% in these experimental conditions to
10 ensure that the measured device current arises from the keratin thin film and not from water
11 condensed on the top of the sample surface. The ionic conductivity reaches about 0.1 µS/cm at
12 80% RH which is consistent with the value extracted from other biopolymers as melanin at 90%
13 RH (10^{-4} - 10^{-3} S/cm) (Wünsche et al., 2015). The ionic conductivity of keratin biofilm can be
14 primary ascribed to the presence of a great amounts of charged amino-acids (*e.g.* cystein-s-
15 sulphonated groups, aspartic acid, glutammic acid, lyisine, arginine and histidine) in the primary
16 structure of the protein (Ordinario et al., 2014). As shown in Figure 2 b, the humidity-dependent
17 ionic conductivity changes induce a repeatable direct current variation, reliable to construct a
18 sensor calibration curve up to RH is equal to 60%. At higher relative humidity we observe a
19 decrease in the current with respect to lower RH levels. The current reduction is likely related to
20 the inefficient injection/extraction of charges at the two electrodes due to the dissolution of the
21 soluble keratin film.
22 Moreover, we used Dielectric Relation Spectroscopy (DRS) technique to investigate the
23 dynamical processes involved in the mechanism of ions transport. Figures 3a and 3b show the
24 real and imaginary parts of dielectric permittivity of the sample, calculated by the equations
25 below (Barsoukov and Macdonald, 2005):
26
27

$$\varepsilon' = \frac{t}{\omega \cdot A \cdot \varepsilon_0} \cdot \left[\frac{Z''}{Z'^2 + Z''^2} \right] \qquad \varepsilon'' = \frac{t}{\omega \cdot A \cdot \varepsilon_0} \cdot \left[\frac{Z'}{Z'^2 + Z''^2} \right] \qquad (3)$$

28

29 where t represents the sample thickness, A is the sample area, ω the angular frequency, ε_0 the
30 electric constant, Z' and Z'' the real and imaginary part of the measured complex impedance,
31 respectively. The real and imaginary parts of the complex dielectric permittivity, respectively ε'
32 reported in Figure 3a and ε'' reported in Figure 3b, show a monotonic decrement with frequency
33 which allows to discriminate between various processes. This monotonic trend is expected for
34 biological systems (Schwan, 1994). In particular, the α relaxation region, which occurs in the
35 frequency range up to 10 Hz, is due to electrode polarization and space charge effects (Radha et
36 al., 2013; Singh et al., 2016). In the frequency range between 10 Hz and 1 MHz the β relaxation
37 region is present that fingerprints the water content in the film (Cicco et al., 2015). At higher
38 frequency, in the γ relaxation region, all the processes are relaxed apart from the reorientation
39 motion of water molecules. Figure 3a shows a higher electrode polarization effect at RH 60%
40 level with respect to RH 20% and 40% levels due to higher hydrogen-bonded water molecules
41 inside KB sensor. When RH is equal to 80% the space charge formation is reduced because
42 keratin dissolution leads to a decreased interfacial polarization effect at the electrode, as we
43 already discussed in the multiple-cycle cyclic voltammetry (Figure 2b). However, the keratin
44 thin film can continue to absorb humidity at RH 80% leading to ionic conductivity enhancement
45 reported in Table 1. This is related to the signal enhancement of ε' in the β relaxation region for

every RH level (Figure 3a). Regarding the imaginary part of the complex dielectric permittivity ε" (Figure 3b), a peak at 1 MHz with an intensity proportional to RH level is observed. We attribute this dielectric contribution at the beginning of the γ relaxation region to the orientational polarization of the water molecules (Cametti et al., 2011). Furthermore, another loss peak appears when RH is 60% at about 3 Hz. A clear shift at 3 kHz when RH reaches 80% is observed. We associate the appearance of this contribution in the imaginary part of the complex dielectric permittivity ε" (Figure 3b) to the relaxation mechanisms in the biopolymer. In fact, a similar dielectric loss-peak shifting toward high frequency values was reported for polymeric electrolytes (Pradhan et al., 2008). The authors discussed that the peak is related to the oscillation of polymer chain segments in specific regions where salt-free microscopic segregation is present so that the gaps left between entangled polymer chains is greater and infilled with the added PEG plasticizer. Our data are consistent with this previous result. In this view, keratin film effectively behaves as a hydrogel, swelling as a function of RH: in this case, the water molecules penetrated in the keratin chains network act as plasticizer agents as already reported for keratin (Chou et al., 2012) and other proteins such as fibroin (Lawrence et al., 2010). Then, the biopolymer chains acquire enhanced flexibility and can move easily under the electric-field oscillation. In general, the peak in ε" spectra which is observed in the β relaxation region of Figure 3b can be used to monitor ion-keratin chain coupling at constant humidity while varying the processing protocols on the keratin thin-films.

3.2. Insoluble diode-like KB sensors

In order to reduce the solubility of keratin thin-films at high humidity levels and thus enabling the fabrication of reliable water-stable KB sensors, we modified the processing of the material. Given that the physical properties of keratin thin-films depend on the conformation of the protein structure in the solid state (McKittrick et al., 2012), specific post-deposition treatments such as water annealing, exposition to organic solvents or dyeing can be implemented to control the biopolymer aggregation or to add new functionalities, as reported for other biomaterials (Cavallini et al., 2015; Jin and Kaplan, 2003).
In our case, water insolubility of KB sensors was obtained by immersion of pure keratin thin film in glutaraldehyde overnight (see the details in Materials & Methods), with a methodology already tested for keratin sponges (Ferroni et al., 2016). The variations detected by means EIS and DRS on the electrical behavior with respect to soluble KB sensor are reported in Figures 3c and 3d. The insolubilizing process leads to increased ionic bulk resistance R_b of the keratin thin film (see the Nyquist plot in Figure 3c). We report the obtained ionic conductivity values in Table 1 for comparison between insoluble and soluble KB sensors. The data indicate that ion transfer under the influence of the electric field is partially inhibited in keratin structure containing glutaraldehyde.
The crosslinking of proteins with glutaraldehyde is generally correlated with the ε-amino group of lysine residues, since they are very reactive as nucleophilic agents. Therefore, the insoluble keratin films contain a reduced number of amino-acid residues involved in the ion transfer. The same behavior was observed by Gorodetsky et al. in the reflectin films (Ordinario et al., 2014). The capacitance plot in Figure S6 in Supporting Information demonstrates that the space charge region is not completely formed with respect to the soluble counterpart at the same humidity and time conditions. In fact, we observe a decreased signal in the α relaxation region together with an intensity increase in the β relaxation region (Figure S6 in Supporting Information, range 10^3-10^5 Hz), reveling the keratin active layer humidity absorption.

To estimate the ability of the insoluble keratin structure to host water molecules, we plot the loss factor as a function of frequency and relaxation time for the soluble and insoluble keratin thin films by using the relation:

$$\omega_{peak} \cdot \tau_r = 1 \qquad (4)$$

where τ_r represents the relaxation time and ω_{peak} the angular frequency related to the peak intensities visible in Figure 3d. Relaxation time is correlated to the ionic polarizability of the biopolymer material at the applied electric field (Shukur et al., 2014): thus, low relaxation time corresponds to high correlation between the permanent dipole moments of water molecules and the electric field oscillations.

This investigation is performed to quantitatively evaluate the grade of influence of the segmental motion of the biopolymer chains on the ion transport given that the mechanism is revealed by dielectric loss plots shown in Figure 3b.

The relaxation time for soluble and insoluble keratin thin films measured in air humidity equal to RH 60% are found to be 0.15 ps and 31.75 ms, respectively. The extracted values are consistent with the conductivity analysis reported in Table 1: slower relaxation times are correlated to a decreased ionic conductivity (Shukla et al., 2014). The peak shifting observed in Figure 3d is comparable to other polymer electrolyte and biopolymer systems where a percentage of plasticizer is added to the chemical recipe (Cicco et al., 2015; Radha et al., 2013). Remarkably, the relaxation time of keratin insoluble structure is comparable to commercial polymer electrolyte (Ravi et al., 2015) allowing this biopolymer to be a competitive insoluble ionic conductor. Figure 4a shows the multiple-cycle cyclic voltammetry at variable relative humidity measured on insoluble KB sensor. As expected, a direct proportionality between the RH and the ion current is finally obtained up to humidity levels higher than the corresponding soluble KB thin-films. The current curve profile is reproducible with a good signal-to-noise ratio. Even though the ionic conductivity is affected by the introduction of glutaraldehyde (ionic conductivity range changes from μS/cm to nS/cm), the correlation between the sensor current output and the humidity levels is finally achieved throughout the entire RH dynamic range while the ionic currents are still well-detectable and can be used as output signal in the sensor. As a final remark, we note that both the soluble and insoluble KB devices are not degrading over time (6 months) in standard environmental conditions thus maintain the expected electrical performance as the pristine devices.

3.3. Melanin-doped KB sensors

In order to increase the ionic conductivity, we doped the pure keratin solution with melanin biopolymer to fabricate a vertical keratin-melanin-based bipole. Since higher ionic conductivity values of hydrated melanin thin film are reported in literature (Wünsche et al., 2015) with respect to keratin, the specific protein organization in melanin biopolymer is expected to increase the number of ordered proton wires to form. Additionally, keratin and melanin are functional compounds already found to coexist in natural hair and in pigmented animal fibers. We used the chemical recipe reported in Materials & Methods section to solubilize melanin and keratin, then the biopolymer composite is obtained by mixing aqueous keratin and melanin solutions in order to obtain a final melanin concentration of 9% wt with respect to keratin.

In Figure 4b we report the Nyquist plots of the measurements performed on the keratin-melanin composite. It is clearly visible the ionic bulk resistance reduction in the keratin-melanin composite: the high-frequency semicircle is correlated to an enhancement of the ionic conductivity with respect to pure keratin regenerated from the ammonia solution (ionic bulk

1 resistance variation from 450 to 50 MΩ). However, the addition of ammonia to the chemical
2 recipe which is necessary to solubilize the melanin biopolymer might lead to different folding of
3 the protein, thereby decreasing the ionic conductivity of the composite, as the less-extended
4 straight-line portion of the Nyquist plot at RH 60% highlights.
5 The transfer of ions in proteins is strictly dependent on the intermolecular packing segmental
6 chains in the solid phase and can be controlled by choosing the right chemical solvent for
7 solubilizing the biopolymers (Brandsburg-zabary et al., 2000). In the specific case, there is the
8 need to find a common solvent to be used for both biopolymers or a process that makes the
9 melanin water soluble. Research into these directions is already in progress.
10
11
12 3.4. Free-standing keratin-based microelectrode array sensor
13
14 Collectively, cross-correlating the sensing functionality assessment (Section 3.1) and the
15 processing optimization and advancement (Section 3.2), we fabricated and validated an
16 integrated and all-keratin made humidity sensor comprised by a transparent, bendable,
17 biocompatible and free-standing substrate and the environment-exposed active layer. Further, we
18 optimized ion injection and extraction by integrating coplanar protodes into KB sensor.
19 As reported in literature (Deng et al., 2013; Hemmatian et al., 2015; Josberger et al., 2016),
20 palladium is an ideal electronic conductor which can be passivated with hydrogen to obtain
21 excellent proton extraction/injection. We performed feasibility tests to verify possible
22 improvements of the current collected by the sensor. The detailed procedure used to obtain the
23 protodes is reported in Materials & Methods section. We performed electrical characterization at
24 constant RH 80%, implementing a larger electrode/protode area with respect to the other
25 fabricated keratin-based bipole (15 mm^2 instead of 6 mm^2 area) in order to guarantee a good
26 signal-to-noise ratio in the collected curves, and thus the straightforward comparison of the
27 electrical figures of merit of the sensor system with and without the passivation of the Pd
28 electrode by hydrogen.
29 The black curve reported in Figure 4c shows the multiple-cycle cyclic voltammetry of hydrated
30 soluble keratin thin film collected for two symmetric palladium electrodes in coplanar
31 configuration. We checked that the humidity-dependence of the electrical current is preserved
32 even in coplanar electrodes configuration with respect to the vertical diode-like configuration
33 (see in Supplementary Information, Figure S7 in Supporting Information). Since the
34 electrode/protode area is larger and the hydration level is fixed at 80% as in the cases of Figures
35 1a, 2b, 4a the decrease of the hysteresis loop in Figure 4c is due to the increase of the
36 geometrical capacity. However, the profile of the cyclic voltammetry curve remains invariant
37 with respect to the case of using gold electrode, revealing the formation of a space charge layer
38 also in the case of Pd electrodes. When Pd electrodes are exposed to hydrogen to form PdHx,
39 protons are efficiently transferred from keratin layer to the electrode according to the reaction
40 $PdH_X \rightarrow Pd + H^+ + e^-$. The output of the electrode functionalization which generates protodes is
41 reported in the red curve in Figure 4c. The electrical current is acquired after few seconds of gas
42 exposition. We observe that the current intensity is enhanced by a factor of about 2 and the curve
43 profile is more linear. A linear current dependence on the applied potential points out that
44 protons do not need to overcome any considerable energy barrier to be injected/collected in/from
45 the active layer (Zhong et al., 2011).
46 Since keratin is a good biopolymer for ion sensing even in coplanar electrode/protode
47 configuration, we fabricated a large-area bendable all-keratin made humidity sensor prototype
48 comprised by an array of KBs. Figures 5 a, b shows the optical images of the fabricated large-
49 area bendable all-keratin made humidity sensor prototype (see in Figure S8 in Supporting
50 Information for the detail of the single device in the array). As can be observed, transparency

and bendability characteristics are effectively obtained. After manufacturing the free-standing bendable substrate, a soluble keratin layer is spin-coated on top of the biopolymeric substrate. Insolubility can be simply obtained by glutaraldehyde immersion as we describe in 3.2 Section.

In the multielectrode array we preferred to implement thermal sublimated gold instead of using palladium electrodes since the latter is more prone to cracking when placed under mechanical stress due to high bending radius.

The electrical curve measured at 60% RH from a single keratin-based bipole of the array is reported in Figure 5c. The gold electrode symmetry is reflected in the cyclic voltammetry as for Figure 4c. The curve shape is similar to the black curve reported in Figure 4c thus showing a decreased capacitive and resistive current due to reduced humidity level (RH 60% vs 80%) and electrode area. In Figure 5d we report the averaged CV curve (correlated with bar errors) obtained from 3 different samples of large-area bendable all-keratin made humidity sensors in order to assess the measure variance of the collected output signal in the fabricated sensor system. As it can be seen from the error bars correlated to the collected data, the results are quite promising in view of the application of the free-standing bendable microelectrode array as a reliable sensor system.

4. Conclusions

In the present work, the intrinsic multifunctionality of keratin structural protein is exploited in order to fabricate the first bendable and free-standing microelectrode array used as humidity sensor that is completely made by the biopolymer.

It is extensively reported that keratin shows the remarkable characteristic of varying the electrical and ionic transport parameters with the uptake of water ions and molecules, thus being a relevant candidate for the realization of a humidity sensors.

In this context, we implemented a selective-chemical doping for suitably functionalizing keratin protein once it is extracted and purified from pristine wool. By doping the keratin solution/thin-films by means of organic compounds, we introduced new functionalities in the biopolymer such as bendability in thin-films and insolubility in high-humidity environment, simply by adding glycerol in solution and immersing thin-films in glutaraldehyde, respectively. Moreover, the blending of keratin solution with higher ion-conductivity biopolymer as melanin and the interfacing of the keratin active layer with Pt-based protodes are implemented for enhancing the proton extraction/injection and transport characteristics in the sensing bipole device.

We demonstrated that the single-device ionic conductivity determined by EIS and CV measurements validates the use of keratin for sensing water molecules and ions even when insolubility feature is displayed, while the working mechanisms of keratin-based bipoles as humidity sensor in controlled and tunable high-humidity levels is extensively discussed by the providing electrical equivalent circuit.

Finally, the entire value-chain of the implementation of keratin biopolymer in ion-sensing applications is reported from protein extraction, to solution processing and sensor system validation in harsh relevant-environment conditions together with preliminary report on stability and repeatability of the sensing performance.

Concluding, considering our latest results on the realization of keratin-based passive patches for drug delivery (Posati et al., 2018), the introduction of structural and chemical-physical features in keratin thin-films as bendability and insolubility in aqueous environments is a key-enabling step for the assessment of the use of multifunctional keratin electroactive membrane into wearable and device system for applications in the biomedical field. In particular, the realized free-standing all-keratin made microelectrode array may meet many of the specifications requested for the development of integrated, portable and even implantable biosensor

(Dragone, R., Grasso, G., Muccini, M., Toffanin, 2017), resulting in a suitable tool for the detection of water ions/molecules to be applied in environment where biocompatibility, sensitiveness and reproducibility are fundamental requisites.

References

Agarwala, S., Lee, J.M., Ng, W.L., Layani, M., Yeong, W.Y., Magdassi, S., 2018. A novel 3D bioprinted flexible and biocompatible hydrogel bioelectronic platform. Biosens. Bioelectron. 102, 365–371. doi:10.1016/j.bios.2017.11.039

Aluigi, A., Sotgiu, G., Torreggiani, A., Guerrini, A., Orlandi, V.T., Corticelli, F., Varchi, G., 2015. Methylene Blue Doped Films of Wool Keratin with Antimicrobial Photodynamic Activity. ACS Appl. Mater. Interfaces 7, 17416–17424. doi:10.1021/acsami.5b04699

Ambrico, M., Ambrico, P.F., Cardone, A., Ligonzo, T., Cicco, S.R., Mundo, R. Di, Augelli, V., Farinola, G.M., 2011. Melanin layer on silicon: An attractive structure for a possible exploitation in bio-polymer based metal-insulator-silicon devices. Adv. Mater. 23, 3332–3336. doi:10.1002/adma.201101358

Baker, H.B., Passipieri, J.A., Siriwardane, M., Ellenburg, M.D., Vadhavkar, M., Bergman, C.R., Saul, J.M., Tomblyn, S., Burnett, L., Christ, G.J., 2017. Cell and Growth Factor-Loaded Keratin Hydrogels for Treatment of Volumetric Muscle Loss in a Mouse Model. Tissue Eng. Part A 23, 572–584. doi:10.1089/ten.tea.2016.0457

Barsoukov, E., Macdonald, J.R., 2005. Impedance Spectroscopy, Impedance Spectroscopy: Theory, Experiment, and Applications. doi:10.1002/0471716243

Benfenati, V., Toffanin, S., Bonetti, S., Turatti, G., Pistone, A., Chiappalone, M., Sagnella, A., Stefani, A., Generali, G., Ruani, G., Saguatti, D., Zamboni, R., Muccini, M., 2013. A transparent organic transistor structure for bidirectional stimulation and recording of primary neurons. Nat. Mater. 12, 672–680. doi:10.1038/nmat3630

Brandsburg-zabary, S., Fried, O., Marantz, Y., Nachliel, E., 2000. Biophysical aspects of intra-protein proton transfer 1458, 120–134.

Cametti, C., Marchetti, S., Gambi, C.M.C., Onori, G., 2011. Dielectric Relaxation Spectroscopy of Lysozyme Aqueous Solutions : Analysis of the δ -Dispersion and the Contribution of the Hydration Water 7144–7153. doi:10.1021/jp2019389

Cavallini, S., Toffanin, S., Chieco, C., Sagnella, A., Formaggio, F., Pistone, A., Posati, T., Natali, M., Caprini, M., Benfenati, V., Di Virgilio, N., Ruani, G., Muccini, M., Zamboni, R., Rossi, F., 2015. Naturally functionalized silk as useful material for photonic applications. Compos. Part B Eng. 71. doi:10.1016/j.compositesb.2014.11.012

Cheng, Z., Chen, X., Zhai, D., Gao, F., Guo, T., Li, W., Hao, S., Ji, J., Wang, B., 2018. Development of keratin nanoparticles for controlled gastric mucoadhesion and drug release. J. Nanobiotechnology 16, 1–13. doi:10.1186/s12951-018-0353-2

Chou, S.F., Overfelt, R.A., Miller, M.E., 2012. Anisotropic mechanical behavior of keratin tissue from quill shells of North American porcupine (Erethizon dorsatum). Mater. Sci. Eng. A 557, 36–44. doi:10.1016/j.msea.2012.05.111

Cicco, S.R., Ambrico, M., Ambrico, P.F., Talamo, M.M., Cardone, A., Ligonzo, T., Di Mundo, R., Giannini, C., Sibillano, T., Farinola, G.M., Manini, P., Napolitano, A., Criscuolo, V., d'Ischia, M., 2015. A water-soluble eumelanin polymer with typical polyelectrolyte behaviour by triethyleneglycol N-functionalization. J. Mater. Chem. C 3, 2810–2816. doi:10.1039/C4TC01997K

Cilurzo, F., Selmin, F., Aluigi, A., Bellosta, S., 2013. Regenerated keratin proteins as potential biomaterial for drug delivery. Polym. Adv. Technol. 24, 1025–1028. doi:10.1002/pat.3168

Deng, Y. et al., 2013. Fabrication of an Electrochemical Biosensor Array for Simultaneous Detection of L-Glutamate and Acetylcholine. J. Biomed. Nanotechnol. 9, 2013.

Deng, Y., Josberger, E., Jin, J., Rousdari, A.F., Helms, B.A., Zhong, C., Anantram, M.P., Rolandi, M., 2013. H + -type and OH - -type biological protonic semiconductors and complementary devices. Sci. Rep. 3. doi:10.1038/srep02481

Dragone, R., Grasso, G., Muccini, M., Toffanin, S., 2017. Portable Bio / Chemosensoristic Devices : innovative Systems for environmental Health and Food Safety Diagnostics. Front. Public Heal. 5, 1–6. doi:10.3389/fpubh.2017.00080

Evans, B.R., O'Neill, H.M., Malyvanh, V.P., Lee, I., Woodward, J., 2003. Palladium-bacterial cellulose membranes for fuel cells. Biosens. Bioelectron. 18, 917–923. doi:10.1016/S0956-5663(02)00212-9

Ferroni, C., Sotgiu, G., Sagnella, A., Varchi, G., Guerrini, A., Giuri, D., Polo, E., Orlandi, V.T., Marras, E., Gariboldi, M., Monti, E., Aluigi, A., 2016. Wool Keratin 3D Scaffolds with Light-Triggered Antimicrobial Activity. Biomacromolecules 17, 2882–2890. doi:10.1021/acs.biomac.6b00697

Hamouche, H., Makhlouf, S., Chaouchi, A., Laghrouche, M., 2018. Sensors and Actuators A : Physical Humidity Sensor Based on Keratin bio Polymer Film. Sensors Actuators A. Phys. 282, 132–141. doi:10.1016/j.sna.2018.09.025

Hemmatian, Z., Miyake, T., Deng, Y., Josberger, E.E., Keene, S., Kautz, R., Zhong, C., Jin, J., Rolandi, M., 2015. Taking electrons out of bioelectronics: bioprotonic memories, transistors, and enzyme logic. J. Mater. Chem. C 3, 6407–6412. doi:10.1039/C5TC00502G

Hod, I., Deria, P., Bury, W., Mondloch, J.E., Kung, C.W., So, M., Sampson, M.D., Peters, A.W., Kubiak, C.P., Farha, O.K., Hupp, J.T., 2015. A porous proton-relaying metal-organic framework material that accelerates electrochemical hydrogen evolution. Nat. Commun. 6, 1–9. doi:10.1038/ncomms9304

Jin, H.J., Kaplan, D.L., 2003. Mechanism of silk processing in insects and spiders. Nature 424, 1057–1061. doi:10.1038/nature01809

Josberger, E.E., Hassanzadeh, P., Deng, Y., Sohn, J., Rego, M.J., Amemiya, C.T., Rolandi, M., 2016. Proton conductivity in ampullae of Lorenzini jelly. Sci. Adv. 2, e1600112. doi:10.1126/sciadv.1600112

Lago, N., Cester, A., Wrachien, N., Natali, M., Quiroga, S.D., Bonetti, S., Barbato, M., Rizzo, A., Benvenuti, E., Benfenati, V., Muccini, M., Toffanin, S., Meneghesso, G., 2016. A physical-based equivalent circuit model for an organic/electrolyte interface. Org. Electron. 35, 176–185. doi:10.1016/j.orgel.2016.05.018

Lago, N., Member, S., Buonomo, M., Member, S., Wrachien, N., Prescimone, F., Natali, M., Muccini, M., Toffanin, S., Cester, A., Member, S., 2018. A General Equivalent Circuit Model for a Metal / Organic / Liquid / Metal System 65, 4555–4562. doi:10.1109/TED.2018.2864682

Lawrence, B.D., Wharram, S., Kluge, J.A., Leisk, G.G., Omenetto, F.G., Rosenblatt, M.I., Kaplan, D.L., 2010. Effect of Hydration on Silk Film Material Properties 7–12. doi:10.1002/mabi.200900294

Li, W. et al., 2018. Reduced Graphene Oxide for Room Temperature Ammonia (NH3) Gas Sensor. J. Nanosci. Nanotechnol. 18, 15563.

M. Folke et al, 2003. Critical review of non-invasive respiratory monitoring in medical care. Med. Biol. Eng. Comput. 377–383.

McKittrick, J., Chen, P.Y., Bodde, S.G., Yang, W., Novitskaya, E.E., Meyers, M.A., 2012. The structure, functions, and mechanical properties of keratin. Jom 64, 449–468. doi:10.1007/s11837-012-0302-8

Miyake, T., Rolandi, M., 2016. Grotthuss mechanisms: from proton transport in proton wires to bioprotonic devices. J. Phys. Condens. Matter 28, 23001. doi:10.1088/0953-8984/28/2/023001

Murphy, E.J., 1976. Ionic conduction in keratin (wool). J. Colloid Interface Sci. 54, 400–408. doi:10.1016/0021-9797(76)90319-2

Ordinario, D.D., Phan, L., Walkup IV, W.G., Jocson, J.M., Karshalev, E., Hüsken, N., Gorodetsky, A.A., 2014. Bulk protonic conductivity in a cephalopod structural protein. Nat. Chem. 6, 596–602. doi:10.1038/nchem.1960

Posati, T., Giuri, D., Nocchetti, M., Sagnella, A., Gariboldi, M., Ferroni, C., Sotgiu, G., Varchi, G., Zamboni, R., Aluigi, A., 2018. Keratin-hydrotalcites hybrid films for drug delivery applications. Eur. Polym. J. 105, 177–185. doi:10.1016/j.eurpolymj.2018.05.030

Pradhan, D.K., Choudhary, R.N.P., Samantaray, B.K., 2008. Studies of dielectric relaxation and AC conductivity behavior of plasticized polymer nanocomposite electrolytes. Int. J. Electrochem. Sci. 3, 597–608. doi:10.1016/j.matchemphys.2009.01.008

Qian, X., Gu, N., Cheng, Z., Yang, X., Wang, E., Dong, S., 2001. Methods to study the ionic conductivity of polymeric electrolytes using a.c. impedance spectroscopy. J. Solid State Electrochem. 6, 8–15. doi:10.1007/s100080000190

Radha, K.P., Selvasekarapandian, S., Karthikeyan, S., Hema, M., Sanjeeviraja, C., 2013. Synthesis and impedance analysis of proton-conducting polymer electrolyte PVA:NH4F. Ionics (Kiel). 19, 1437–1447. doi:10.1007/s11581-013-0866-5

Ravi, M., Song, S., Gu, K., Tang, J., Zhang, Z., 2015. Electrical properties of biodegradable poly(∈-caprolactone): Lithium thiocyanate complexed polymer electrolyte films. Mater. Sci. Eng. B Solid-State Mater. Adv. Technol. 195, 74–83. doi:10.1016/j.mseb.2015.02.003

Robinson, J.T., Pietron, J.J., Blue, B., Perkins, F.K., Josberger, E., Deng, Y., Rolandi, M., 2017. Electrical and electrochemical characterization of proton transfer at the interface between chitosan and PdHX. J. Mater. Chem. C 5, 11083–11091. doi:10.1039/c7tc03215c

Rouse, J.G., Van Dyke, M.E., 2010. A review of keratin-based biomaterials for biomedical applications. Materials (Basel). 3, 999–1014. doi:10.3390/ma3020999

Schwan, H.P., 1994. Electrical properties of tissues and cell suspensions: mechanisms\nand models. Proc. 16th Annu. Int. Conf. IEEE Eng. Med. Biol. Soc. 70–71. doi:10.1109/IEMBS.1994.412155

Shukla, N., Thakur, A.K., Shukla, A., Marx, D.T., 2014. Ion conduction mechanism in solid polymer electrolyte: An applicability of almond-west formalism. Int. J. Electrochem. Sci. 9, 7644–7659.

Shukur, M.F., Ithnin, R., Kadir, M.F.Z., 2014. Electrical properties of proton conducting solid biopolymer electrolytes based on starch-chitosan blend. Ionics (Kiel). 20, 977–999. doi:10.1007/s11581-013-1033-8

Singh, R., Singh, P.K., Singh, V., Bhattacharya, B., 2016. Agarose Biopolymer Electrolytes : Ion Conduction Mechanism and Dielectric Studies.

Tachibana, A., Furuta, Y., Takeshima, H., Tanabe, T., Yamauchi, K., 2002. Fabrication of wool keratin sponge scaffolds for long-term cell cultivation. J. Biotechnol. 93, 165–170. doi:10.1016/S0168-1656(01)00395-9

Tang, L., Sierra, J.O., Kelly, R., Kirsner, R.S., Li, J., 2012. Wool-derived keratin stimulates human keratinocyte migration and types IV and VII collagen expression. Exp. Dermatol. 21, 458–460. doi:10.1111/j.1600-0625.2012.01505.x

Toffanin, S., Benfenati, V., Pistone, A., Bonetti, S., Koopman, W., Posati, T., Sagnella, A., Natali, M., Zamboni, R., Ruani, G., Muccini, M., 2013. N-type perylene-based organic semiconductors for functional neural interfacing. J. Mater. Chem. B 1, 3850. doi:10.1039/c3tb20555j

Toffanin, S., Kim, S., Cavallini, S., Natali, M., Benfenati, V., Amsden, J.J., Kaplan, D.L., Zamboni, R., Muccini, M., Omenetto, F.G., 2012. Low-threshold blue lasing from silk fibroin thin films. Appl. Phys. Lett. 101. doi:10.1063/1.4748120

Wünsche, J., Deng, Y., Kumar, P., Di Mauro, E., Josberger, E., Sayago, J., Pezzella, A., Soavi, F., Cicoira, F., Rolandi, M., Santato, C., 2015. Protonic and electronic transport in hydrated thin films of the pigment eumelanin. Chem. Mater. 27, 436–442. doi:10.1021/cm502939r

Yadav, R., Fedkiw, P.S., 2012. Analysis of EIS Technique and Nafion 117 Conductivity as a Function of Temperature and Relative Humidity. J. Electrochem. Soc. 159, B340–B346. doi:10.1149/2.104203jes

Zhong, C., Deng, Y., Roudsari, A.F., Kapetanovic, A., Anantram, M.P., Rolandi, M., 2011. A polysaccharide bioprotonic field-effect transistor. Nat. Commun. 2, 475–476. doi:10.1038/ncomms1489

Zhou, X., Cheng, X., Zhu, Y., Elzatahry, A.A., Alghamdi, A., Deng, Y., Zhao, D., 2018. Ordered porous metal oxide semiconductors for gas sensing 29, 405–416. doi:10.1016/j.cclet.2017.06.021
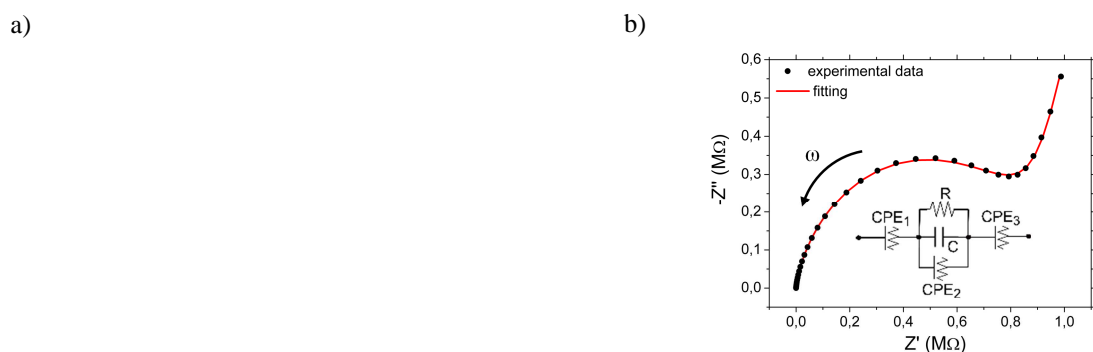
Figures

a) b)

Figure 1. (a) Soluble KB sensor, one night in glove-box then, ambient humidity sensing by single-cycle cyclic voltammetry. The maximum standard deviation is 0.5 nA in y-axis. (b) Nyquist plot for quantitative fitting from soluble KB sensor in ambient air humidity. Inset: electrical equivalent circuit.
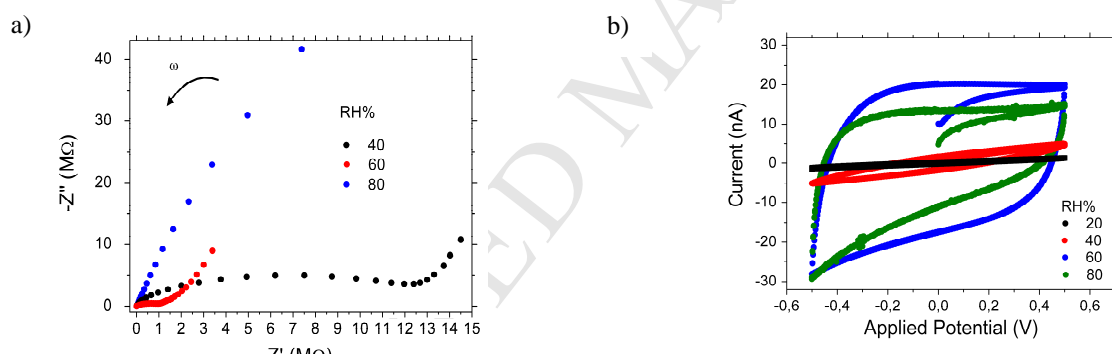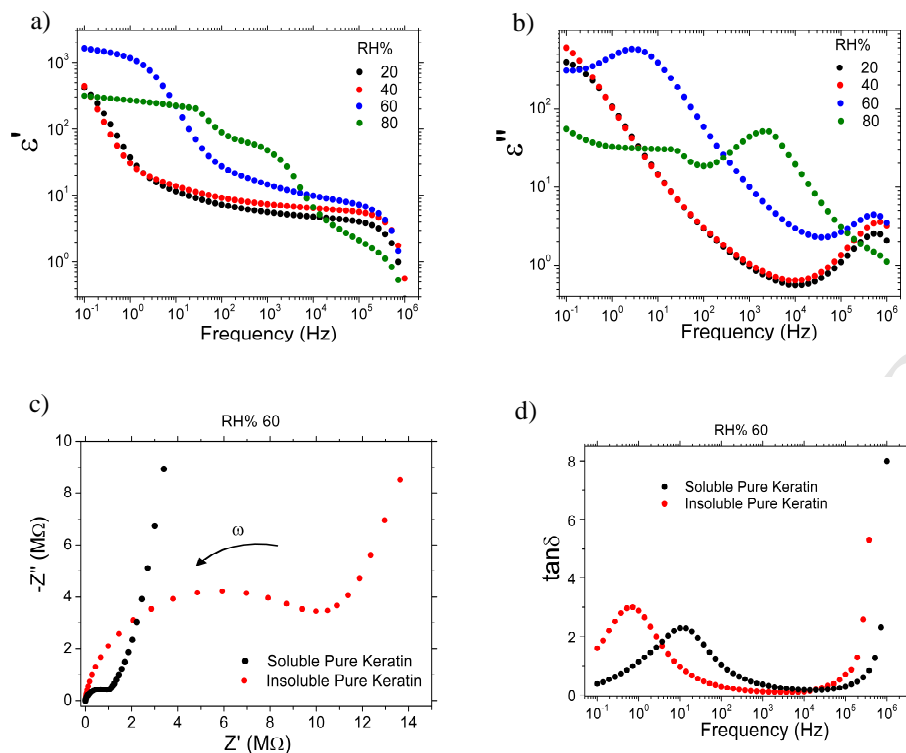
a) b)

Figure 2. (a) Nyquist plots of soluble KB sensor at variable RH. The maximum standard deviation is 0.1 MΩ in x-axis and 0.06 MΩ in y-axis. (b) Multiple-cycle cyclic voltammetry of soluble KB sensor at variable RH.

Table 1. Device lectrical figures of merit dependence on RH (soluble *vs* insoluble)

RH%	d (nm)	S (cm^2)	R_b (Ω) Soluble	R_b (Ω) Insoluble	δ (S/cm) Soluble	δ (S/cm) Insoluble
40	450	0.06	10^7	-	$75 \cdot 10^{-12}$	-
60	450	0.06	10^6	10^7	$0.75 \cdot 10^{-9}$	$0.75 \cdot 10^{-10}$
80	450	0.06	6000	$160 \cdot 10^3$	$0.13 \cdot 10^{-6}$	$4.69 \cdot 10^{-9}$

Figure 3. (a) DRS on soluble KB sensor at variable RH: dielectric constants. (b) DRS on soluble KB sensor at variable RH: dielectric losses. (c) Nyquist plots of KB sensor at constant RH: soluble *vs* insoluble comparison. The maximum standard deviation is 5.5 MΩ in x-axis and 3.6 MΩ in y-axis for the insoluble KB sensor. (d) Loss factors of KB sensor at constant RH, soluble *vs* insoluble comparison.
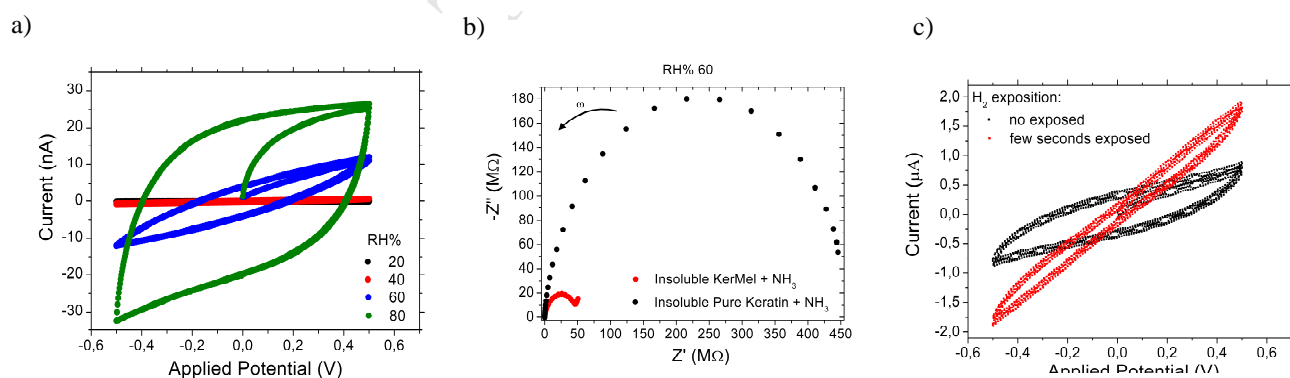
Figure 4. (a) Multiple-cycle cyclic voltammetry at variable RH from insoluble keratin. The maximum standard deviation is 4.6 nA in the y-axis. (b) Nyquist plot from biopolymer-based capacitors at constant RH, pure soluble keratin *vs* keratin-melanin composite; (c) Multiple-cycle cyclic voltammetry from soluble keratin at constant RH, Pd electrodes *vs* PdHx protodes.
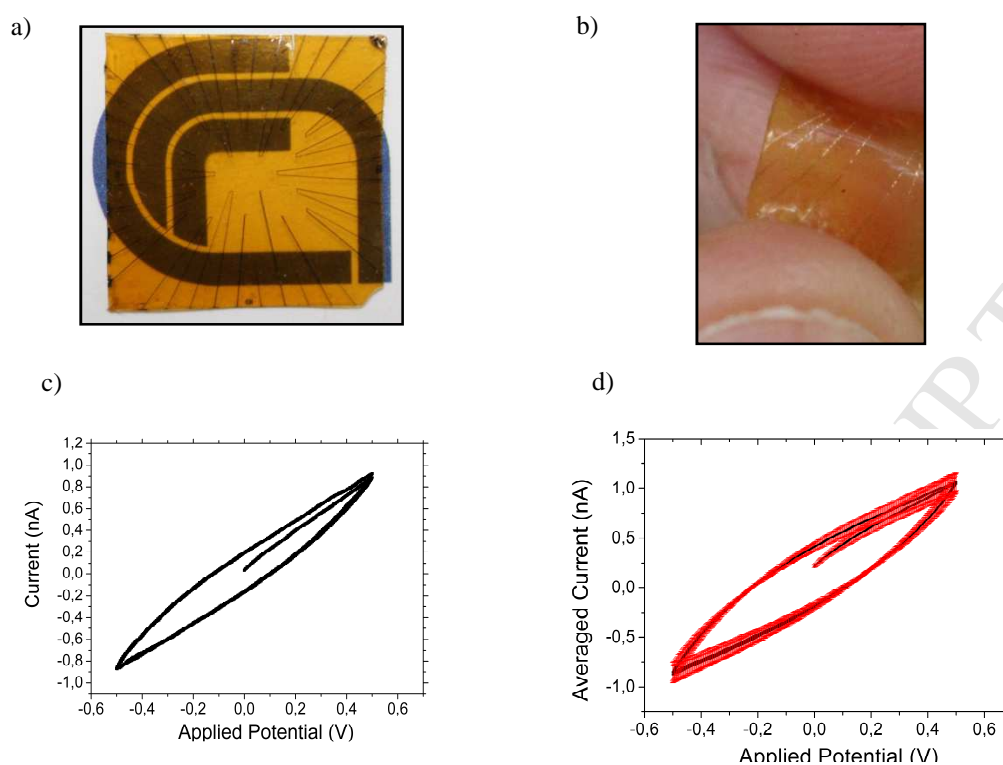
a)

b)

c)

d)

Figure 5. (a) Free-standing insoluble keratin-based microelectrode array superimposed to CNR symbol to show transparency; (b) bending of the sensor free-standing insoluble keratin-based microelectrode array by using fingers; (c) Multiple-cycle cyclic voltammetry from free-standing soluble keratin-based microelectrode array at constant 60% RH. (d) Multiple-cycle cyclic voltammetry as in (c) from 3 different sensor system samples for providing information about measure variance (maximum standard deviation of 0.1 nA in the y-axis).

Engineering of keratin functionality for the realization of bendable all-biopolymeric micro-electrode array as humidity sensor

M. Natali*[a], A. Campana[a], T. Posati[b], E. Benvenuti[a], F. Prescimone[a], D.O. Sanchez Ramirez[c], A. Varesano[c], C. Vineis[c], R. Zamboni[b], M. Muccini[a], A. Aluigi[b], S. Toffanin*[a]

[a] Consiglio Nazionale delle Ricerche (CNR)— Istituto per lo Studio dei Materiali Nanostrutturati (ISMN), Via P. Gobetti 101, 40129 Bologna, Italy
[b] Consiglio Nazionale delle Ricerche (CNR)— Istituto per la Sintesi Organica e la Fotoreattività (ISOF), Via P. Gobetti 101, 40129 Bologna, Italy
[c] Consiglio Nazionale delle Ricerche (CNR), Istituto di Sistemi e Tecnologie Industriali Intelligenti per il Manifatturiero Avanzato (STIIMA), Corso Giuseppe Pella 16, 13900 Biella, Italy

Highlights

- A microelectrode array was successfully fabricated onto a transparent, bendable, insoluble, biocompatible and suitable-chemically modified free-standing substrate made of keratin biopolymer

- Naturally-extracted keratin biomaterial was implemented as active layer in microelectrode array engineered in coplanar electrode architecture, preserving in a thin-film form the hygroscopic properties of pristine wool keratin that permit humidity sensing

- Cyclic voltammetry, electrical impedance spectroscopy and dielectric relaxation spectroscopy were performed in order to electrochemically characterize the sensors to define proper figures of merits and assess material-related sensing properties

Engineering of keratin functionality for the realization of bendable all-biopolymeric micro-electrode array as humidity sensor

M. Natali*[a], A. Campana[a], T. Posati[b], E. Benvenuti[a], F. Prescimone[a], D.O. Sanchez Ramirez[c], A. Varesano[c], C. Vineis[c], R. Zamboni[b], M. Muccini[a], A. Aluigi[b], S. Toffanin*[a]

[a] Consiglio Nazionale delle Ricerche (CNR)— Istituto per lo Studio dei Materiali Nanostrutturati (ISMN), Via P. Gobetti 101, 40129 Bologna, Italy

[b] Consiglio Nazionale delle Ricerche (CNR)— Istituto per la Sintesi Organica e la Fotoreattività (ISOF), Via P. Gobetti 101, 40129 Bologna, Italy

[c] Consiglio Nazionale delle Ricerche (CNR), Istituto di Sistemi e Tecnologie Industriali Intelligenti per il Manifatturiero Avanzato (STIIMA), Corso Giuseppe Pella 16, 13900 Biella, Italy

Credit Author Statement

Dr. Marco Natali: Conceptualization, Investigation, Data curation, Writing - original draft

Dr. A. Campana: Conceptualization, Investigation

Dr. T. Posati: Investigation, Methodology

Dr. E. Benvenuti: Investigation

Dr. F. Prescimone: Investigation

Dr. D.O. Sanchez Ramirez: Investigation

Dr. A. Varesano: Investigation, Methodology

Dr. C. Vineis: Investigation, Methodology

Dr. R. Zamboni: Writing - review & editing

Dr. M. Muccini: Writing - review & editing

Dr. A. Aluigi: Investigation, Methodology, Validation

Dr. S. Toffanin: Conceptualization, Data curation, Writing - original draft, Writing - review & editing, Supervision, Validation, Funding acquisition

Declaration of interests

☒ The authors declare that they have no known competing financial interests or personal relationships that could have appeared to influence the work reported in this paper.

☐The authors declare the following financial interests/personal relationships which may be considered as potential competing interests: